Chinese Chemical Letters 34 (2023) 107437

Contents lists available at ScienceDirect

Chinese Chemical Letters

journal homepage: www.elsevier.com/locate/cclet

Controllable synthesis of MnO_2/iron mesh monolithic catalyst and its significant enhancement for toluene oxidation

Meijuan Qi[a,b], Zhe Li[a,b], Zhang Zhang[c], Yanshan Gao[a,b,*], Qiang Wang[a,b,*]

[a] Beijing Key Lab for Source Control Technology of Water Pollution, College of Environmental Science and Engineering, Beijing Forestry University, Beijing 100083, China

[b] Engineering Research Center for Water Pollution Source Control & Eco-remediation, College of Environmental Science and Engineering, Beijing Forestry University, Beijing 100083, China

[c] Beijing Municipal Ecological and Environmental Monitoring Center, Beijing 100048, China

ARTICLE INFO

Article history:
Received 12 January 2022
Revised 16 February 2022
Accepted 12 April 2022
Available online 19 April 2022

Keywords:
Toluene oxidation
Iron mesh monoliths catalysts
MnO_2
Resistance properties
Reaction mechanism

ABSTRACT

A series of monolithic MnO_2/iron mesh (IM) catalysts for oxidation of toluene were successfully prepared by using *in situ* hydrothermal growth. MnO_2 can grow firmly on the IM substrates surface with a shedding rate of only 0.14%. Due to the highest O_{ads} and high-valent Mn^{4+} and Fe^{3+} elements, the temperature at 50% and 90% toluene conversion ($T_{50\%}$ and $T_{90\%}$) was 252 and 265 °C, respectively for the best performance catalyst (hydrothermal temperature of 80 °C, hydrothermal time of 12 h, and precursor manganese ion concentration of 0.03 mol/L). The catalysts also presented good water resistance and cycle performance. *In-situ* DRIFTS results suggesting that toluene was first rapid transformed into the reaction intermediate species (benzoate species) and then converted to CO_2 and H_2O. Therefore, this work provides a new direction for the research and application of IM-based monolithic catalysts.

Volatile organic compounds (VOCs) have detrimental effects on environment and human health, not only due to they are important precursors of fine particulate matter ($PM_{2.5}$) and ozone (O_3), but also because of their toxicity, mutagenesis and carcinogenicity [1,2]. Catalytic oxidation is considered to be an efficient technique for VOCs abatement due to its advantages of high efficiency, low reaction temperature, low energy consumption and no secondary pollution, *etc.* [3]. Development of high efficiency and cost-effective non-noble metal catalyst for VOCs oxidation at low temperature is important.

Moreover, in practical applications, powder catalysts have the problem of high pressure drop, difficult separation and easy to lose, which are difficult to be applied to real industrial production. Monolithic catalysts such as ceramic monoliths (mostly made of cordierite and currently the most used) can avoid these problems to a large extent [4]. Unfortunately, poor attachment stability between the honeycomb ceramic carrier and powder lead to the loss of surface-active species during the reaction process, which reduces the catalytic efficiency and limits the application. Besides, the ceramic supports also have some drawback such as low mechanical strength, uneven internal heat distribution and inhomogeneous distribution of surface catalyst powder.

In order to overcome those shortcomings, metallic monoliths catalysts with high mechanical strength and plasticity, good thermal conductivity and mass transfer ability, appropriate roughness and porosity were developed [5]. At present, the application of metal-supported monoliths catalysts mainly includes Ni foam, alloys, aluminum foil, and wire mesh, *etc.* Compared with other metallic monoliths catalysts, iron mesh (IM)-based catalysts have connected three-dimensional channel structure, which cannot only serve as catalyst support, but also provide iron atoms. In our previous work, IM-supported vertically aligned Co-Fe layered double oxides was prepared and compared with traditional cordierite-based catalysts. The IM based catalysts showed good catalytic activity and water resistance [6], suggesting IM can be a promising carrier for monolithic catalysts.

In this work, in order to further improve the low temperature catalytic performance, manganese oxide was *in-situ* growth on the surface of IM by using one-step hydrothermal method, which can not only achieve the stable decoration of manganese precursor on the surface of IM, but also ensure the uniform dispersion of active components. The hydrothermal conditions, catalytic activity, thermal stability, water resistance, cycle performance and the toluene

* Corresponding authors at: Beijing Key Lab for Source Control Technology of Water Pollution, College of Environmental Science and Engineering, Beijing Forestry University, Beijing 100083, China.

E-mail addresses: yanshan_gao@bjfu.edu.cn (Y. Gao), qiangwang@bjfu.edu.cn (Q. Wang).

https://doi.org/10.1016/j.cclet.2022.04.035
1001-8417/

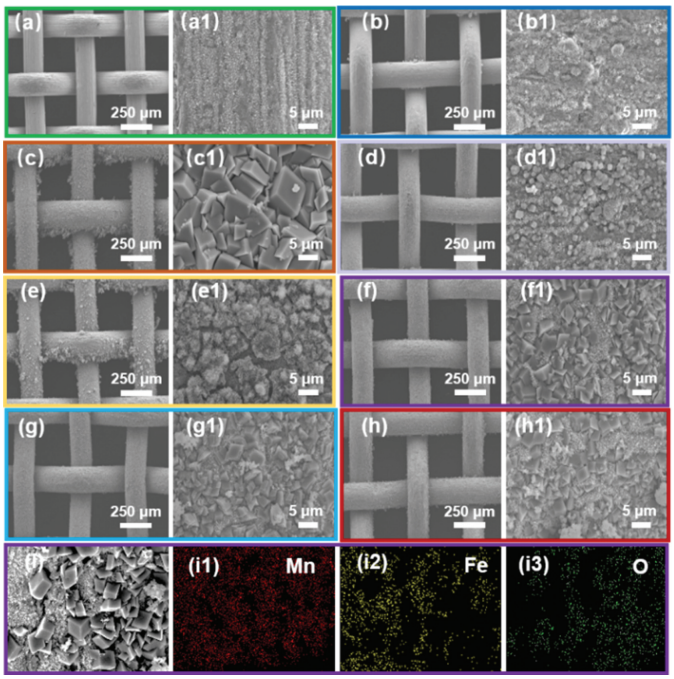

Fig. 1. (a) SEM images of pure iron mesh; SEM images of MnO_2/IM monolithic catalysts at hydrothermal temperature of (b) 60 °C, (c) 80 °C, (d) 100 °C, (e) 120 °C, (f) 140 °C, (g) 160 °C, (h) 180 °C, (i) elemental mappings results of MnO_2/IM monolithic catalyst with hydrothermal temperature of 140 °C.

reaction process of the MnO_2/IM monolithic catalyst were investigated systematically.

The crystalline phase of the catalysts was illustrated by X-ray diffraction (XRD) analyses (Fig. S1 in Supporting information). After growing MnO_2 on IM surface, the obtained MnO_2/IM-*T* monolithic catalysts with different hydrothermal temperature (Fig. S1a) depicted diffraction peaks at $2\theta = 28.68°$, 37.33°, 42.82° and 56.65° were corresponded to (110), (101), (111) and (211) lattice planes, respectively, which were consistent with β-MnO_2 (pyrolusite) crystalline phase (JCPDS No. 24-0735), suggesting that MnO_2 successfully grown on IM. Simultaneously, a part of the iron element in the IM were transformed into Fe_3O_4 through high temperature hydrothermal and calcination (JCPDS No. 75-0033). Similarly, MnO_2/IM-80-*t* and *n*-MnO_2/IM-80-12 catalysts were similar with those of MnO_2/IM-*T* (Figs. S1b and c), indicating that the hydrothermal conditions within the experimental range showed no significant effect on crystal structure of the monoliths samples.

Scanning electron microscope (SEM) showed that the pure IM presented a rough surface (Fig. 1a), which is conducive to the growth of other substances. After hydrothermal reaction, the IM was coated with *in situ* grown iron and manganese oxides as shown in Figs. 1b–h. The morphologies of Fe and Mn oxides covered on the monolithic catalyst surface was mainly cubic structure and flake. The morphologies of the Fe and Mn oxides on the surface of IM were obviously different with different hydrothermal temperature conditions. Similarly, suitable hydrothermal time ($t = 12$ h) can make crystal phase develop completely, make the reaction more thorough and produce more cubic structure (Fig. S2 in Supporting information). Fig. S3 (Supporting information) also showed that the concentration of manganese ion in the hydrothermal solution play an important role in the development of cubic structure, and the best precursor concentration was 0.03 mol/L.

For a clearer observation, the MnO_2/IM monolithic catalyst prepared at 140 °C was selected for Energy dispersive spectrometer (EDS) mapping as shown in Fig. 1i. The cubic structure on IM surface was composed of rich Mn and O elements, and the vertical flake shape was composed of rich Fe and O elements, all the elementals were highly dispersed. Therefore, a layer of flake Fe_3O_4 was formed on the surface of the iron mesh, and then cubic structure MnO_2 were grown on top of it.

Table 1
Surface Mn, Fe, and O elements molar ratios for MnO_2/IM monolithic catalyst with different hydrothermal temperature.

Samples	Surface element ratio		
	$Mn^{4+}/(Mn^{3+}+Mn^{2+})$	Fe^{3+}/Fe^{2+}	O_{ads}/O_{latt}
MnO_2/IM-60	0.53	0.44	0.42
MnO_2/IM-80	0.76	0.88	0.52
MnO_2/IM-100	0.74	0.83	0.43
MnO_2/IM-120	0.57	0.75	0.45

Fig. S4 (Supporting information) shows the hydrogen temperature programmed reduction experiments (H_2-TPR) curves of the catalysts prepared under different hydrothermal conditions. In general, MnO_2 was reduced in steps of $Mn^{4+} \rightarrow Mn^{3+} \rightarrow Mn^{2+}$ [7]. For all samples, the reduction peak observed at lower temperature (280~400 °C) was mainly the reduction process of Mn^{4+} to $Mn^{3+}$and Mn^{3+} was further reduced to Mn^{2+}. Significantly, compared with the catalysts prepared at other hydrothermal temperatures, the temperature required for Mn^{4+} reduction to Mn^{3+} moved to a lower direction for MnO_2/IM-80 monolithic catalyst (Fig. S4a). Also, among the samples prepared at different time, the reduction temperature for Mn^{4+} to Mn^{3+} of MnO_2/IM-12 and MnO_2/IM-24 samples were basically the same, but the intensity of the reduction peak of MnO_2/IM-12 samples was higher (Fig. S4b). At the same, the Mn^{4+} could be reduced to Mn^{3+} at ~280 °C for MnO_2/IM-0.03 sample, while the reduction temperature of others was approximately at 400 °C. The reduction peaks observed at higher temperature (about 530 °C) correspond to the co-reduction processes of $Mn^{3+} \rightarrow Mn^{2+}$ and $Fe^{3+} \rightarrow Fe^{2+} \rightarrow Fe$. And the reduction peak at about 600 °C was further reduction of $Fe^{2+} \rightarrow Fe$.

The surface $Mn^{4+}/(Mn^{3+}+Mn^{2+})$, Fe^{3+}/Fe^{2+} and O_{ads}/O_{latt} were summarized in Table 1. The full X-ray photoelectron spectroscopy (XPS) spectrum of the samples indicated the presence of Mn, Fe and O elements. MnO_2/IM-80 showed the strongest Mn 2p peak and the weakest Fe 2p peak (Fig. S5a in Supporting information). The Mn $2p_{3/2}$ spectra of the catalyst could be decomposed into three spin orbital lines with binding energies of 641.3, 641.7 and 643.4 eV, attributed to Mn^{2+}, Mn^{3+}, and Mn^{4+} species, respectively (Fig. S5b in Supporting information) [8]. It is well known that the coexistence of Mn^{4+} and Mn^{3+} facilitates the migration and conversion of electrons, which is beneficial to the redox properties of the samples, thus improving their catalytic activity [9]. The $Mn^{4+}/(Mn^{3+}+Mn^{2+})$ molar ratio decreased with the trend: MnO_2/IM-80 (0.76) > MnO_2/IM-100 (0.74) > MnO_2/IM-120 (0.57) > MnO_2/IM-60 (0.53). This sequence suggests that different hydrothermal temperatures affect the $Mn^{4+}/(Mn^{3+}+Mn^{2+})$ molar ratio on IM surface, further suggesting that the MnO_2/IM-80 catalyst has the best redox properties, which is consistent with the H_2-TPR results.

The surface molar ratio of Mn^{4+}/Mn^{3+} also further affects the lattice oxygen (O_{latt}) and adsorbed oxygen (O_{ads}) species on the MnO_2 surface, such as O^-, O^{2-} and O_2^{2-}. In Fig. S5c (Supporting information), the O 1s XPS spectrum of the samples can be divided into three peaks corresponding to lattice oxygen (O_{latt}, 530 ± 0.2 eV), surface adsorbed oxygen (O_{ads}, 531.3 ± 0.2 eV) and adsorbed OH groups and water molecule (O_{OH}, 533 eV) [10]. The O_{ads}/O_{latt} ration decreased in the order of MnO_2/IM-80 (0.52) > MnO_2/IM-120 (0.45) > MnO_2/IM-100 (0.43) > MnO_2/IM-60 (0.42). According to the relevant literature, surface adsorbed oxygen has

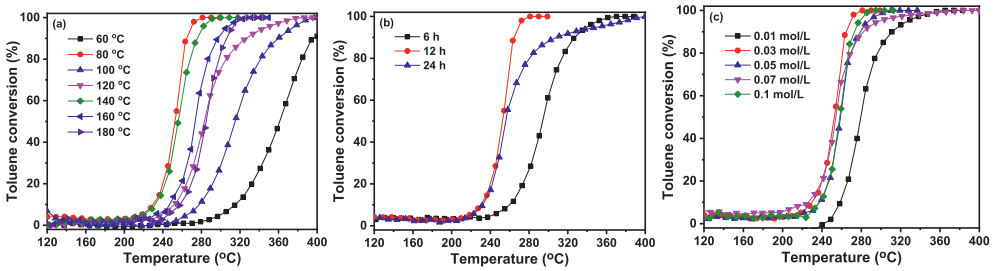

Fig. 2. Catalytic oxidation of toluene over MnO_2/IM monolithic catalysts at different (a) hydrothermal temperatures, (b) hydrothermal times and (c) precursor concentrations.

higher mobility than lattice oxygen, which makes MnO_2/IM-80 more active in the reaction [11,12].

In addition, the Fe 2p peaks in Fig. S5d (Supporting information) could be split into four peaks and two satellite peaks. The peaks of Fe $2p_{3/2}$ could be divided into two peaks of Fe^{3+} (712.9 eV) and Fe^{2+} (710.7 eV) [6]. This indicated that the iron in IM was oxidized to Fe_3O_4, which was consistent with the XRD results. Fe^{3+}/Fe^{2+} molar ratio of the MnO_2/IM-80 (0.88) was higher than that of MnO_2/IM-60 (0.44), MnO_2/IM-100 (0.83), MnO_2/IM-120 (0.75). In conclusion, MnO_2/IM-80 has the highest number of O_{ads} and high-valent Mn^{4+} and Fe^{3+} elements, which can be presumed to have the best catalytic performance.

The toluene catalytic activity showed a trend of increasing and then decreasing with the increasing of hydrothermal temperatures (Fig. 2), which was consistent with the XPS analysis described above. Different hydrothermal time and precursor concentration also had some effect on the toluene oxidation. The results can be concluded that the MnO_2/IM monolithic catalyst prepared at a hydrothermal temperature of 80 °C, hydrothermal time of 12 h, and precursor manganese ion concentration of 0.03 mol/L had the best catalytic activity for toluene oxidation, which $T_{50\%}$ and $T_{90\%}$ (the temperature at 50% and 90% toluene conversion) were 252 °C and 265 °C, respectively. Furthermore, combined with SEM-EDS analysis, it can be concluded that MnO_2 with a cubic morphology on the surface of IM is the main active component for toluene oxidation.

Additionally, Table S1 (Supporting information) summarizes the catalytic performance for toluene oxidation over different monolithic catalysts. Compared with the previous results, the MnO_2/IM monolithic catalyst prepared in this paper presents better catalytic activity of toluene when taking into account the different experimental conditions. The three-dimensional porous network of the IM matrix is beneficial to the formation of the active component of MnO_2, which not only shows good mass transfer performance for the reactant molecule, but also increases the contact between the reactant and the surface site [5]. Beside, it is well known that due to the exposure of active interfaces and enrichment of oxygen vacancies, MnO_2 can enhance the toluene oxidation activity [13]. In addition, the shedding rate of MnO_2/IM monolithic catalyst was only 0.14%, suggesting that this *in situ* growth technique makes the metal oxide bond firmly to the substrate, which is more conducive to practical industrial applications.

The thermal stability of the best performance 0.03-MnO_2/IM-80-12 monolithic catalysts calcined at 400∼700 °C was investigated (Fig. 3a). $T_{50\%}$ and $T_{90\%}$ of MnO_2/IM-400 was 252 °C and 265 °C. When the calcination temperature was 500 °C, 600 °C and 700 °C, the $T_{50\%}$ increased to 305 °C, 313 °C and 340 °C while $T_{90\%}$ increased to 332 °C, 333 °C and 368 °C, respectively, which probably due to partial sintering of the active component or loss on the surface of the catalyst [14].

From XRD analysis (Fig. 3b), the main manganese product of 400 °C calcination was β-MnO_2. After the calcination temperature raised to 500∼700 °C, the product gradually transformed into Mn_2O_3 (JCPDS No. 41–1442). Moreover, Fe_3O_4 transformed into Fe_2O_3 crystal phase compared with MnO_2/IM-400 (JCPDS No. 39–1346). And with the increasing of calcination temperature, the intensity of Mn_2O_3 and Fe_2O_3 diffraction peaks gradually increased. Since MnO_2 showed remarkable toluene oxidation activity than Mn_2O_3, which mainly attribute to strong redox ability and active oxygen species storage [15]. Therefore, MnO_2 phase on the surface of iron mesh changed to Mn_2O_3 phase is one of the main reasons for the decrease of catalyst activity at high calcination temperatures.

Water vapor could cover and block the active sites of the catalyst [16]. After introduced water vapor in the airflow, the conversion rate of toluene decreased slightly from 95% to 89% after continuing the reaction for 1 h (Fig. 3c), which may be related to the competitive adsorption of toluene with water molecules on the surface of catalyst [17]. Subsequently, the toluene conversion was immediately restored when water vapor was removed. As a result, water vapor can be released from the surface of the catalyst in time, that is, the deactivation was reversible. This result indicated that the MnO_2/IM catalyst present certain water resistance, which may be attributed to the poor water absorption of the IM substance and the active component MnO_2 [18–20].

Fig. 3d shows the cyclic test of 0.03-MnO_2/IM-80–12 catalyst for toluene catalytic oxidation. During each cycle, the catalyst was slowly increased from room temperature to 360 °C and keep it at 3 h. In the 1st, 2nd, 3rd and 4th cycle, the $T_{90\%}$ value was 281, 301, 307 and 317°C, respectively. The catalytic performance was only slightly reduced after 4 cycles. The active components on the surface of IM may fall off due to continuous scouring of the airflow, leading to the reduction of the active components, thus reducing the catalytic activity [21]. Thus, the as-prepared 0.03-MnO_2/IM-80–12 monolithic catalyst is promising for toluene degradation because of its low cost, high catalytic activity, low shedding rate and excellent water resistance.

Fig. S6 (Supporting information) exhibits the time-resolved *in-situ* diffuse reflectance infrared fourier transform spectroscopy (*in-situ* DRIFTS) spectra of toluene adsorption and oxidation with time on 0.03-MnO_2/IM-80–12 sample at 260 °C. The peak at around 1603 cm^{-1} was attributed to the stretching vibration of aromatic ring, and the band at 3057, 3028, 1452 and 1496 cm^{-1} were assigned to the phenylic C-H stretching vibration and the bending vibration peaks of asymmetric methyl groups, respectively. The peaks intensity increased with the increasing of reaction time, which indicated that toluene was adsorbed on the surface of the catalyst [22–24]. Simultaneously, the peak at 1405 and 1540 cm^{-1}, respectively corresponded to the symmetric C-O tensile vibration peak and the asymmetric C-O tensile vibration peak of benzoic acid, indicating that the benzoate species (C_6H_5-COOH) were the main intermediates product in the oxidation of toluene over 0.03-MnO_2/IM-80–12 monolithic catalyst [25,26]. Moreover, all the *in-situ* DRIFTS showed the final product of CO_2 at around 2342 and 2360 cm^{-1}, and the intensities gradually increased with the increasing of detection time [27,28]. The results showed that the lattice oxygen on the surface of 0.03-MnO_2/IM-80–12 monolithic cat-

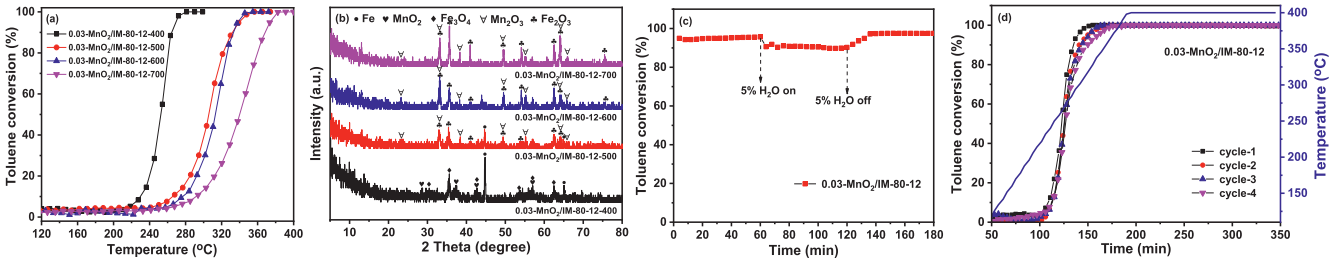

Fig. 3. (a) Catalytic oxidation of toluene and (b) XRD of 0.03-MnO_2/IM-80–12 monolithic catalysts at different calcination temperatures, (c) effect of 5 vol% H_2O on toluene combustion and (d) cyclic test of 0.03-MnO_2/IM-80–12 monolithic catalyst.

alyst could participate in the degradation of absorbed toluene and oxidation of benzoic acid and other intermediated, but the intermediates could not be fully oxidized due to the lack of sustainable reactive oxygen species [29].

In toluene oxidation process, toluene characteristic peaks (1591, 1508 and 3065 cm^{-1}) and benzoic acid species characteristic peaks (1413 and 1558 cm^{-1}) can be observed after 20 vol% oxygen was introduced for 60 min. In addition, the oxidation path of toluene on the surface of 0.03-MnO_2/IM-80–12 monolithic catalyst could be quickly converted to intermediate species benzoic acid, and eventual oxidation to CO_2 (2318 and 2365 cm^{-1}) and H_2O. No characteristic peak of benzaldehyde species was observed during toluene oxidation, which may be the reason for the rapid conversion of benzaldehyde species into benzoic acid species. The intensity of toluene and benzoic acid characteristic peaks did not decrease significantly with the increasing of time, even after introduced 20 vol% oxygen, indicating that toluene and benzoic intermediates species absorbed on the surface of the catalyst reached saturation. Therefore, the reaction path of toluene on the catalyst surface can be inferred: the rapid conversion of toluene to the intermediate product benzoic acid and eventual transformed to CO_2 and H_2O.

In this work, one-step *in situ* hydrothermal method was used to make MnO_2/IM monolithic catalysts. The MnO_2 can grow evenly and firmly on the IM surface by adjusting the hydrothermal conditions, which shedding rate was only 0.14%. The obtained catalysts (prepared at a hydrothermal temperature of 80 °C, hydrothermal time of 12 h, and precursor manganese ion concentration of 0.03 mol/L) presented excellent toluene oxidation performance with a $T_{90\%}$ value of 265 °C (GHSV = 60,000 mL g^{-1} h^{-1}), this can be attributed to the unique three-dimensional network structure of the iron mesh carrier. XPS also proved that MnO_2/IM-80 presented the highest O_{ads} and high-valent Mn^{4+} and Fe^{3+} elements, which is benefit for catalytic reaction. High temperature may cause MnO_2 phase on the surface of IM transformed to Mn_2O_3, thus leading to a relatively low catalytic activity. Beside, due to the hydrophobicity of IM, the MnO_2/IM monolithic catalyst presented certain water resistance under 5 vol% water vapor. And the catalytic performance was only slightly reduced after 4 cycles. Thus, the as-prepared MnO_2/IM monolithic catalyst in this work is promising for the practical oxidation of toluene.

Declaration of competing interest

The authors report no declarations of interest.

Acknowledgments

This work was supported by the Fundamental Research Funds for the Central Universities (No. 2021ZY79), Beijing Municipal Education Commission through the Innovative Transdisciplinary Program "Ecological Restoration Engineering" (No. GJJXK210102), National Natural Science Foundation of China (Nos. 42075169, U1810209), National Key R&D Program of China (No. 2021YFE0110800) and Chinese-Serbian collaboration project (No. 451-03-1205/2021-09).

Supplementary materials

Supplementary material associated with this article can be found, in the online version, at doi:10.1016/j.cclet.2022.04.035.

References

[1] R.J. Huang, Y. Zhang, C. Bozzetti, et al., Nature 514 (2014) 218–222.
[2] Y. Guo, M. Wen, G. Li, T. An, Appl. Catal. B: Environ. 281 (2021) 119447.
[3] C. He, J. Cheng, X. Zhang, et al., Chem. Rev. 119 (2019) 4471–4568.
[4] S.G. Ronald, M. Heck, R.J. Farrauto, Chem. Eng. J. 82 (2001) 149–156.
[5] O. Sanz, E.D. Banús, A. Goya, et al., Catal. Today 296 (2017) 76–83.
[6] T. Xue, R. Li, Y. Gao, Q. Wang, Chem. Eng. J. 384 (2020) 123284.
[7] N.S. Portillo-Vélez, R. Zanella, Chem. Eng. J. 385 (2020) 123848.
[8] L. Liu, J. Li, H. Zhang, et al., J. Hazard. Mater. 362 (2019) 178–186.
[9] Y. Wu, Y. Lu, C. Song, et al., Catal. Today 201 (2013) 32–39.
[10] W. Tang, X. Wu, D. Li, et al., J. Mater. Chem. A 2 (2014) 2544–2554.
[11] X. Lin, S. Li, H. He, et al., Appl. Catal. B: Environ. 223 (2018) 91–102.
[12] H. He, X. Lin, S. Li, et al., Appl. Catal. B: Environ. 223 (2018) 134–142.
[13] N. Huang, Z. Qu, C. Dong, et al., Appl. Catal. A: Gen. 560 (2018) 195–205.
[14] W.B. Li, W.B. Chu, M. Zhuang, J. Hua, Catal. Today 93–95 (2004) 205–209.
[15] W. Yang, Y. Peng, Y. Wang, et al., Appl. Catal. B: Environ. 278 (2020) 119279.
[16] P. Liu, H. He, G. Wei, et al., Appl. Catal. B: Environ. 182 (2016) 476–484.
[17] S.M. Saqer, D.I. Kondarides, X.E. Verykios, Appl. Catal. B: Environ. 103 (2011) 275–286.
[18] T. Xue, R. Li, Z. Zhang, et al., J. Environ. Sci. China 96 (2020) 194–203.
[19] Y. Lyu, C. Li, X. Du, et al., Fuel 262 (2020) 116610.
[20] Y. Dong, J. Zhao, J.Y. Zhang, et al., Chem. Eng. J. 388 (2020) 124244.
[21] L. Chen, G. Liu, N. Feng, et al., Appl. Surf. Sci. 467-468 (2019) 1088–1103.
[22] S. Mo, Q. Zhang, Y. Sun, et al., J. Mater. Chem. A 7 (2019) 16197–16210.
[23] Y. Wang, J. Wu, G. Wang, et al., Appl. Catal. B: Environ. 285 (2021) 119873.
[24] E. Yu, J. Li, J. Chen, et al., J. Hazard. Mater. 388 (2020) 121800.
[25] H. Zhang, S. Sui, X. Zheng, et al., Appl. Catal. B: Environ. 257 (2019) 117878.
[26] C. Dong, H. Wang, Y. Ren, Z. Qu, J. Environ. Sci. China 104 (2021) 102–112.
[27] B. Jiang, K. Xu, J. Li, et al., J. Hazard. Mater. 405 (2021) 124203.
[28] P. Wang, J. Wang, X. An, et al., Appl. Catal. B: Environ. 282 (2021) 119560.
[29] X. Chen, X. Chen, S. Cai, et al., Appl. Surf. Sci. 475 (2019) 312–324.